International Journal of Engineering and Science Invention (IJESI)
ISSN (Online): 2319-6734, ISSN (Print): 2319-6726
www.ijesi.org ||Volume 15 Issue 7 July 2026 || PP 48-59

ADMET predictions, Molecular Dynamics and Molecular Docking of 1-[3-Methyl-5-(2,6,6-trimethyl-cyclohex-1-enyl)-4,5-dihydro-pyrazol-1-yl]-ethanone [$C_{15}H_{26}N_2O$]

Tanveer Hasan[a], Sayed Hasan Mehdi[b#], Tazeem[b], Syed Asad Ali[a] and Nazia Kazmi[c]

[a]*Deptt. of Physics, Shia P.G. College, Lucknow-226020, India.*
[b]*Deptt. of Chemistry, Shia P.G. College, Lucknow-226020, India.*
[c]*Deptt. of Zoology, Shia P.G. College, Lucknow-226020, India.*
[#]*Corresponding author. Email: mehdi.sayed@gmail.com*

Abstract
This work is based on the study of molecular docking, molecular dynamics and ADMET parameters of 1-[3-Methyl-5-(2,6,6-trimethyl-cyclohex-1-enyl)-4,5-dihydro-pyrazol-1-yl]-
ethanone ($C_{15}H_{26}N_2O$) [MTDPE], a molecule reported to possess several bioactive properties. The compound's equilibrium geometry has been derived using the DFT-B3LYP/LANL2DZ approach. The drug-likeness and ADMET factors were calculated to examine their medicinal properties. The proteins 5YDJ and 6E1C have been analyzed through molecular docking with the compound MTDPE to explore potential bioactive properties. A molecular dynamics simulation lasting 100 ns was executed, evaluating models via RMSD, RMSF, Rg, PC1-PC2-PLOT metrics, SASA, Protein-Ligand Contacts other bonding parameters.
Keywords: *Molecular Dynamics; Ethanone ($C_{15}H_{26}N_2O$); ADMET; DFT; Molecular docking.*

I. Introduction

Over the years, pyrazoles have enjoyed a prominent place in heterocyclic chemistry largely due to the wide range of biological activity associated with this class of compounds. The title molecule was synthesized by our research group and reported for its synthesis, Characterization and Cholinesterase enzymes inhibitory activity [1]. Pyrazoles are simple aromatic compounds of heterocyclic diazole series characterized by 5 membered ring structures composed of 3 carbon atoms and 2 nitrogen atoms in adjacent positions, and to the unsubstituted parent compound. Pyrazoles display a broad spectrum of biological activities. Pyrazoles and its derivatives are used for their antitumor [2-4], antimicrobial [3,5,6], antioxidants [3], antiproliferative [7], anti-inflammatory [3,8] and neuroprotective [9] activities. The title compound's "1-[3-Methyl-5-(2,6,6-trimethyl-cyclohex-1-enyl)-4,5-dihydro-pyrazol-1-yl]-ethanone ($C_{15}H_{26}N_2O$)" [MTDPE] equilibrium geometry has been derived and examined using the DFT-B3LYP/LANL2DZ approach using Gaussian 09 software. This optimized geometry was then use to compute other parameters. The model molecular structure was obtained employing Gaussview 6. Molecular dynamics (MD) simulations investigate the time-dependent physical, structural, and thermodynamic properties of chemical drugs and their interactions with biological targets [10]. The molecular docking analysis is employed by researchers with scoring functions to screen vast digital databases of chemical compounds in silico via computer simulation. This rapidly filters out inactive molecules and identifies potential "hit" compounds that fit into a target's active site of the compound.

II. Computational Methods

Gaussian 09 software was used to perform quantum chemical calculations for the molecule NPU [11]. In this work, DFT is used in conjunction with the Lee, Yang, and Parr correlation functional and Becke's three-parameter hybrid exchange functional B3LYP [12-14]. In order to calculate vibrational frequencies, electric and electronic parameters, Fukui functions, etc., the optimal geometry has been obtained. The GaussView 6.0 software application was used to create the model molecular structure[15]. SWISSADME and preADME online program was used to evaluate ADMET and pharmacokinetic properties [16]. The Google Colaboratory platform was used for all of the molecular dynamics simulations [17]. Docking calculations were conducted using Autodock Vina tools 4.2.6 and PyMol software [18,19].

III. Result and Discussion

3.1. Geometry Optimization

Initially the geometry of the title compound was optimized employing DFT method, and this optimized parameters, were used calculate other parameters of the molecule. Figure 1 shows ortep view of the title compound's MTDPE developed by x-ray data, whereas figure 2 displays the optimal configuration produced from the Gauss View 6.

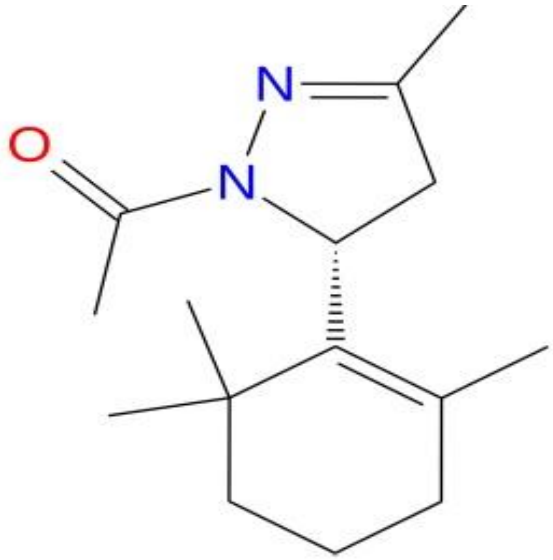

Fig. 1: Model molecular structure of developed by molecular dynamics simulation

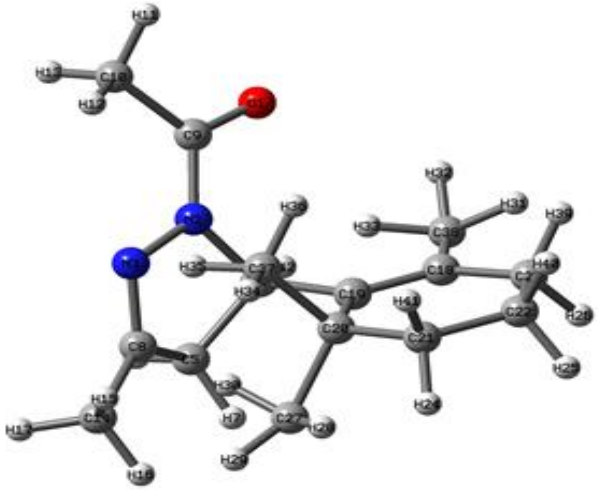

Fig. 2: Model molecular structure as viewed from Gaussview 6

3.2 Molecular Dynamics Simulations

3.2.1 RMSD Analysis

The root mean square deviation (RMSD) method was utilized to analyze the structural properties of ligands within the active site of proteins. Figure 3(a) and (b) present the RMSD graphs for the studied ligand, MTDPE, concerning the two protein receptors, 5YDJ and 6E1C, respectively. All protein frames are first aligned on the reference frame backbone, and then the RMSD is calculated based on the atom selection. Monitoring the RMSD of the protein can give insights into its structural conformation throughout the simulation. RMSD analysis can indicate if the simulation has equilibrated — its fluctuations towards the end of the simulation are around some thermal average structure. Changes of the order of 1-3 Å are perfectly acceptable for small, globular proteins. Changes much larger than that, however, indicate that the protein is undergoing a large conformational change during the simulation. It is also important that the simulation

converges — the RMSD values stabilize around a fixed value. In the above plot, 'Lig fit Prot' shows the RMSD of a ligand when the protein-ligand complex is first aligned on the protein backbone of the reference and then the RMSD of the ligand heavy atoms is measured. If the values observed are significantly larger than the RMSD of the protein, then it is likely that the ligand has diffused away from its initial binding site.

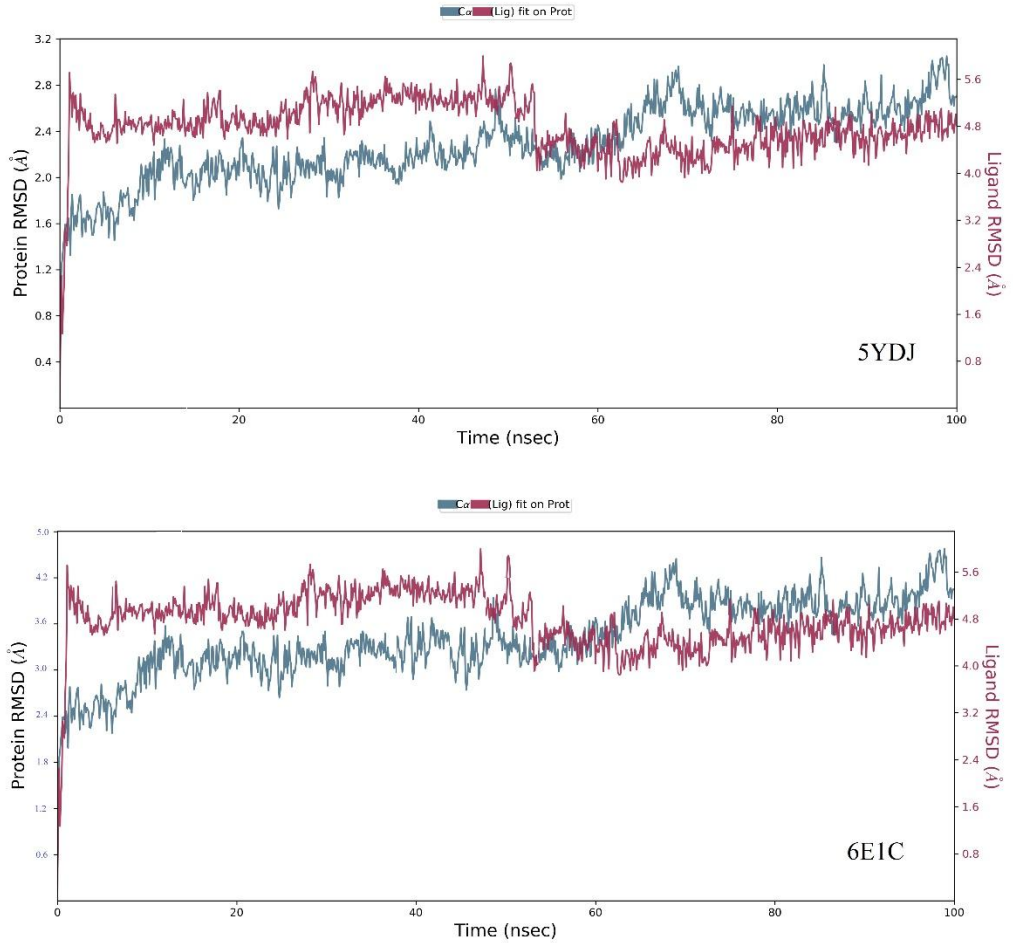

Fig.3. RMSD fluctuations of ligand MTDPE with the two-protein receptors

For the ligand-protein receptor pairs MTDPE-5YDJ and MTDPE-6E1C, the RMSD values for proteins 5YDJ and 6E1C (shown in blue) start at 0.8 Å and increase to 3.0 Å, subsequently oscillating between 2.4 Å and 3.0 Å, ultimately stabilizing at around 2.6 Å. For the ligand MTDPE, the RMSD fluctuation begins at 0.6 Å, varies between 5.8 and 4.6 Å, and ultimately stabilizes at 4.8 Å. For the MTDPE-6E1C complex, the RMSD value for the protein receptor 6E1C begins at 0.6 Å, reaches a maximum of σ = 4.2 Å, and varies between 1.8.4 and 5.6 Å before ultimately stabilizing at 5.4 Å at 100 ns.

3.2.2 Root Mean Square Fluctuations

The Root Mean Square Fluctuation (RMSF) is useful for characterizing local changes along the protein chain. On this plot, peaks indicate areas of the protein that fluctuate the most during the simulation. Typically, it is observed that the tails (N- and C-terminal) fluctuate more than any other part of the protein. Secondary structure elements like alpha helices and beta strands are usually more rigid than the unstructured part of the protein, and thus fluctuate less than the loop regions. Figures 4(a) and (b) illustrate the root mean square (RMS) variations of the title compound MTDPE interacting with the two receptor proteins, 5YDJ and 6E1C, respectively. The graphical data indicate that the RMS fluctuations peak at 3.0 Å around the residue index with 60-75 residue indices and fluctuates between 0.5 to 2.5 Å and finally settles around 3.0 Å for both receptors. Both protein receptors demonstrate analogous structural behavior affected by the ligand MTDPE, leading to similar contributions to their RMS fluctuations. The ligand RMSF illustrates the ligand's fluctuations segmented by atom, aligning with the 2D structure in the upper panel. The ligand RMSF can provide information on how ligand fragments engage with the protein and their entropic contribution to the binding process. In the lower panel, the 'Fit Ligand on Protein' line

indicates the ligand variations in relation to the protein. The protein-ligand complex is initially aligned along the protein backbone, after which the ligand RMSF is assessed on the heavy atoms of the ligand.

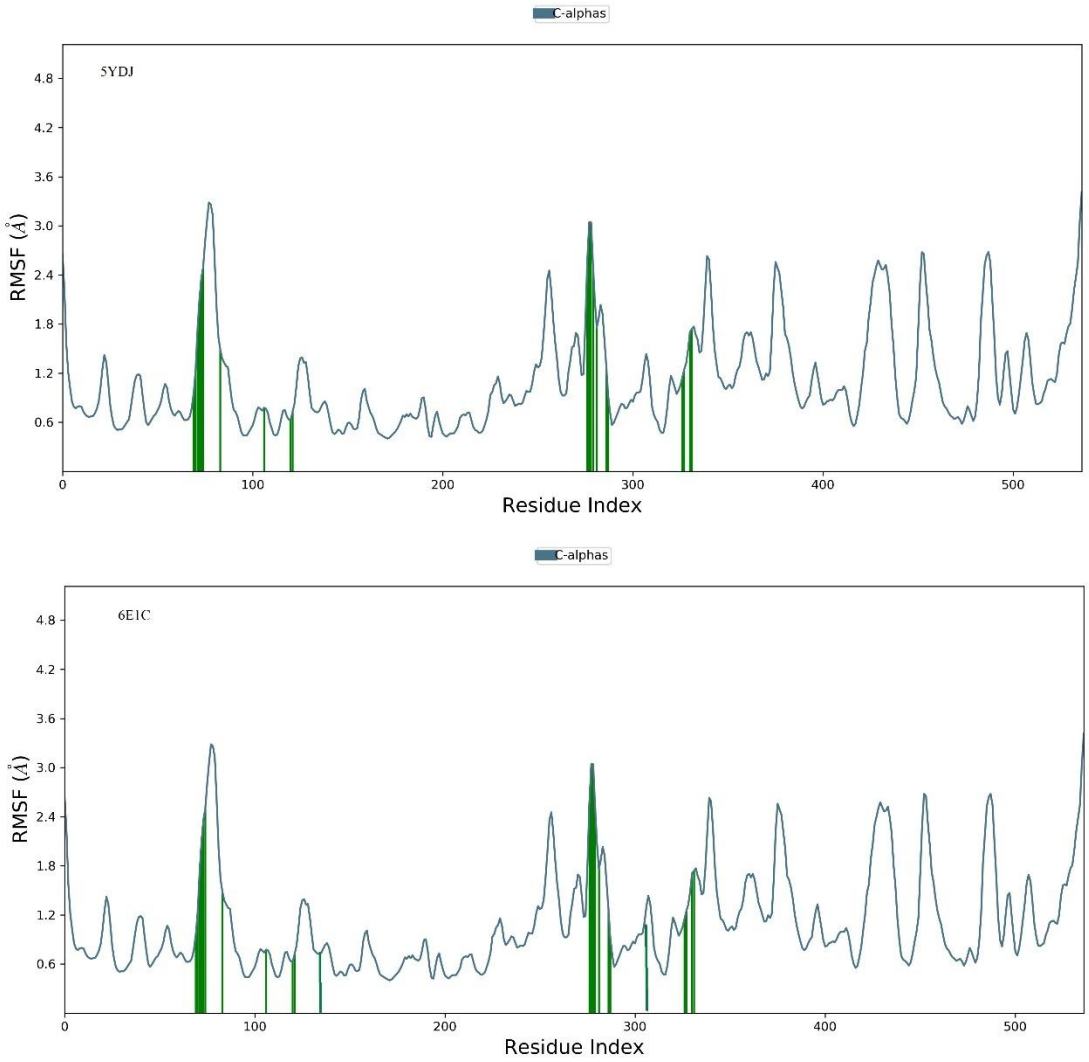

Fig 4. RMSF fluctuations of ligand MTDPE with the two-protein receptor

3.2.3 Radius of Gyration (R_g)

The radius of gyration (Rg) serves to determine the structural compactness of a protein structure. The visual displays of Rg can aid in evaluating the stiffness of a protein structure. During the 100 ns simulation period, properly folded proteins exhibit fairly consistent values, whereas misfolded or unstable proteins reveal fluctuations. The 2D graphs in figures 5(a) and (b) show that Rg varied until 90 ns, after which the Rg values for protein receptors 5YDJ and 6E1C stabilized at 2.88 Å because of the ligand MTDPE.

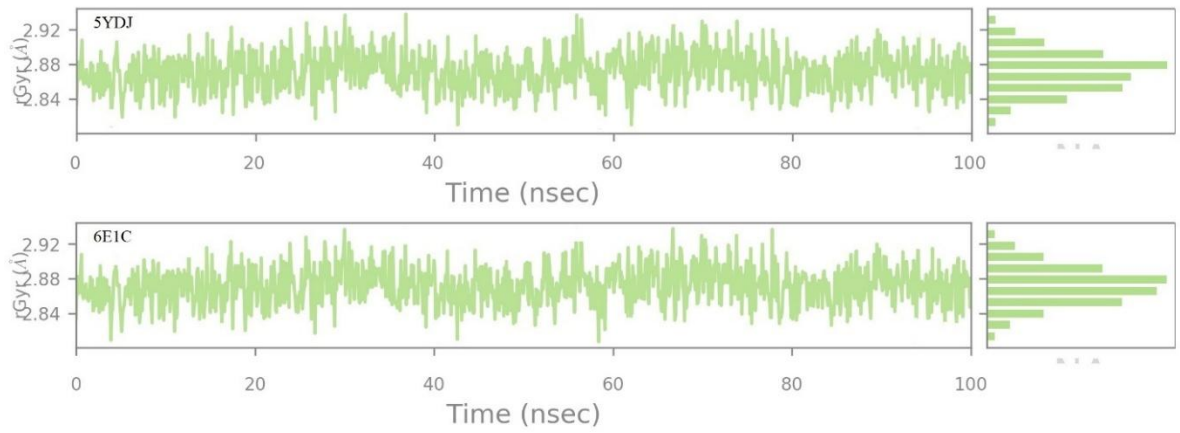

Fig. 5. Radius of gyration R_g of ligand MTDPE with the two-protein receptors

3.2.4 Solvent Accessible Surface Area (SASA)

Solvent Accessible Surface Area (SASA) gives the information about surface area of a molecule accessible by a water molecule. The SASA schematic of the ligand MTDPE with two proteins are shown in figure 6.

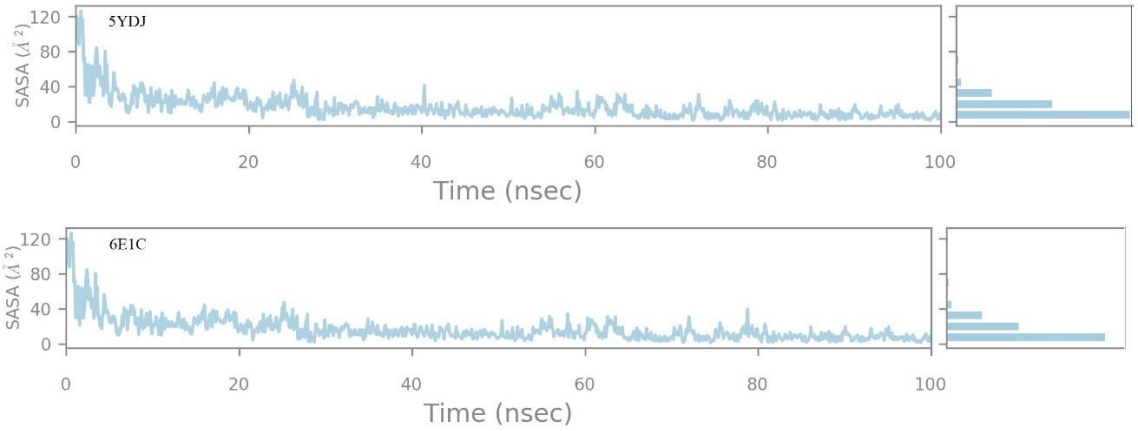

Fig. 6: SASA of the ligand MTDPE with two proteins

3.2.5. Protein-Ligand Contacts

Protein interactions with the ligand can be monitored throughout the simulation. These interactions can be categorized by type and summarized, as shown in the plot in fig 7. Protein-ligand interactions (or 'contacts') are categorized into four types: Hydrogen Bonds, Hydrophobic, Ionic and Water Bridges. Each interaction type contains more specific subtypes, which can be explored through the 'Simulation Interactions Diagram' panel. The stacked bar charts are normalized over the course of the trajectory: for example, a value of 0.7 suggests that 70% of the simulation time the specific interaction is maintained. Values over 1.0 are possible as some protein residue may make multiple contacts of same subtype with the ligand.

Hydrogen Bonds: (H-bonds) play a significant role in ligand binding. Consideration of hydrogen-bonding properties in drug design is important because of their strong influence on drug specificity, metabolization and adsorption. Hydrogen bonds between a protein and a ligand can be further broken down into four subtypes: backbone acceptor; backbone donor; side-chain acceptor; side-chain donor. The current geometric criteria for protein-ligand H-bond is: distance of 2.5 Å between the donor and acceptor atoms (D—H···A); a donor angle of $^{3}120°$ between the donor-hydrogen-acceptor atoms (D—H···A); and an acceptor angle of $^{3}90°$ between the hydrogen-acceptor-bonded-atom atoms (H···A—X).

Hydrophobic contacts: fall into three subtypes: p-Cation; p-p; and Other, non-specific interactions. Generally, these types of interactions, involve a hydrophobic amino acid and an aromatic or aliphatic group on the ligand, but we have extended this category to also include p-Cation interactions. The current geometric criteria for hydrophobic interactions is as follows: p-Cation — Aromatic and charged groups within 4.5 Å; p-p — Two aromatic groups stacked face-to-face or face-to-edge; Other — A non-specific hydrophobic sidechain within 3.6 Å of a ligand's aromatic or aliphatic carbons.

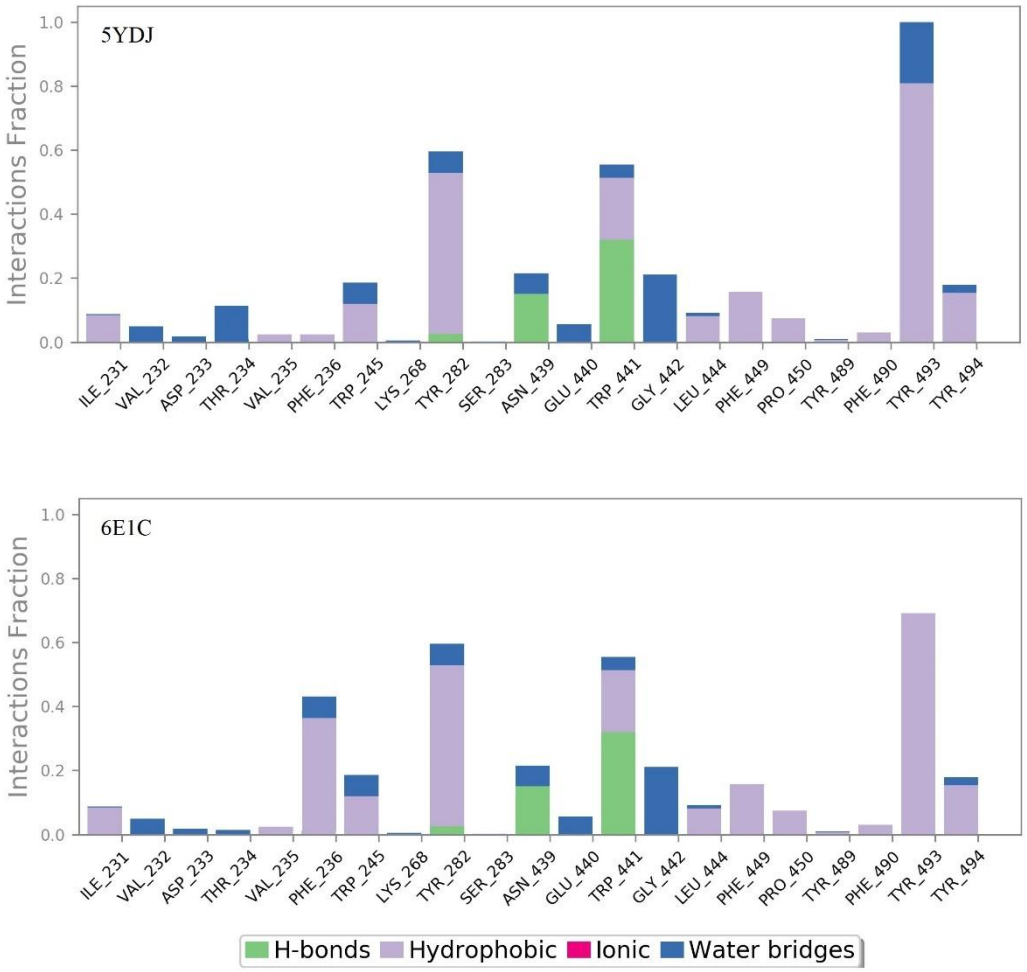

Fig. 7: Protein-Ligand Contacts for title ligand and two receptors 5YDJ and 6E1C

Ionic interactions: or polar interactions, are between two oppositely charged atoms that are within 3.7 Å of each other and do not involve a hydrogen bond. We also monitor Protein-Metal-Ligand interactions, which are defined by a metal ion coordinated within 3.4 Å of protein's and ligand's heavy atoms (except carbon). All ionic interactions are broken down into two subtypes: those mediated by a protein backbone or side chains.
Water Bridges: are hydrogen-bonded protein-ligand interactions mediated by a water molecule. The hydrogen-bond geometry is slightly relaxed from the standard H-bond definition. The current geometric criteria for a protein-water or water-ligand H-bond are: a distance of 2.8 Å between the donor and acceptor atoms (D—H···A); a donor angle of [3]110° between the donor-hydrogen-acceptor atoms (D—H···A); and an acceptor angle of [3]90° between the hydrogen-acceptor-bonded-atom atoms (H···A—X).

3.3 Molecular docking

For docking analysis, the target proteins were chosen utilizing the way2drug.com online target prediction tool [20]. The proteins of interest (PDB ID: "5YDJ and 6E1C") were sourced from the Protein Data Bank [21]. The protein "5YDJ" falls in the type of protein *Transferase (Kinase)*.

It belongs to a unique family of alpha-kinases that regulate cellular myosin assembly and cell motility by phosphorylating specific threonine residues on the myosin heavy chain. The other protein belongs to the "Oxidoreductase (Diheme Peroxidase-like superfamily)". It belongs to the *bCcP/MauG superfamily*. It acts as an enzyme likely responsible for the post-translational modification of molecules involved in binding or handling bacterial copper. The proteins, ligands, and grid maps were set up for docking with Auto Grid and Auto Dock tools, and docking simulations were performed using the Autodock Vina 4.2.6 software. 2D interaction profile images of the ligand MTDPE with proteins 5YDJ and 6E1C were generated using PYMOL software [22, 23]. Examination of docking in PYMOL for MTDPE with the 5YDJ receptor protein revealed two hydrogen bonds with the residue O682 at a distance of 2.5 Å each, as illustrated in figure 8(a), showing an interaction energy of -

7.0 Kcal/mol. The docking analysis for MTDPE with the 6E1C protein receptor similarly revealed one hydrogen bond with the K318 residue at a distance of 3.3 Å, showing an interaction energy of -6.6 Kcal/mol.

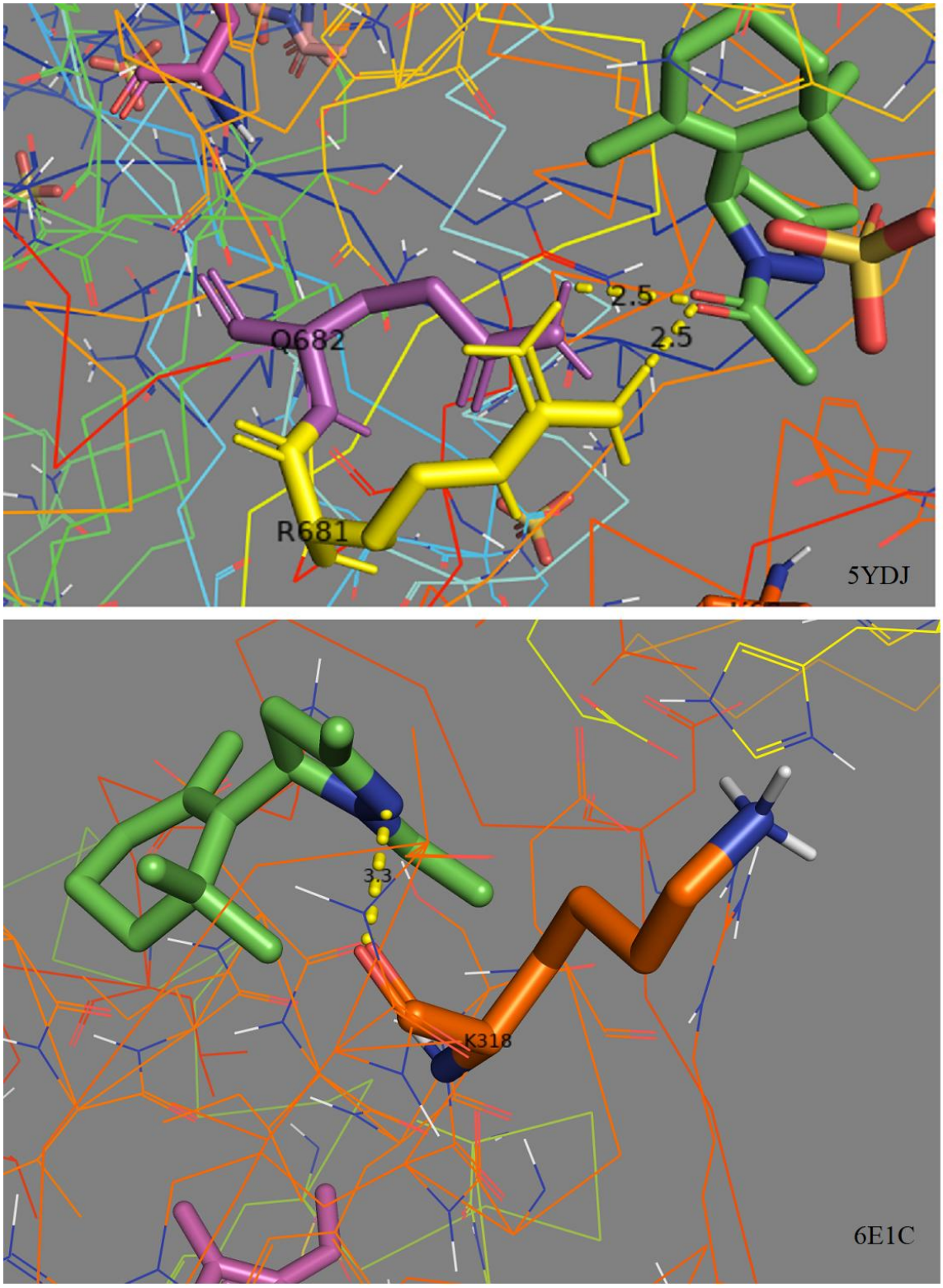

Fig. 8: Molecular docking poses as obtained by PyMol software

3.4. Characteristics of Drug Likeness and ADME Profiles

ADME (Absorption, Distribution, Metabolism, and Excretion) parameters, which are the four core processes that describe how a pharmaceutical drug moves through and is processed by the body. These properties

form the foundation of pharmacokinetics—the study of what the body does to a drug over time. Understanding them helps scientists design safe, effective medications and determine the right dosages.

Table I: Drug Likeness, ADME parameters etc. of MTDPE compound

S.No.	Physicochemical Properties		S.No.	Ali Class	Soluble
1	Molecule	MTDPE	25	Silicos-IT LogSw	-3.15
2	Molecular Formula	C15H24N2O	26	Silicos-IT Solubility (mg/ml)	1.75E-01
3	MW	248.36	27	Silicos-IT Solubility (mol/l)	7.03E-04
4	#Heavy atoms	18	28	Silicos-IT class	Soluble
5	#Aromatic heavy atoms	0		Pharmacokinetics	
6	Fraction Csp3	0.8	29	GI absorption	High
7	#Rotatable bonds	2	30	BBB permeant	Yes
8	#H-bond acceptors	2	31	Pgp substrate	No
9	#H-bond donors	0	32	CYP1A2 inhibitor	No
10	MR	81	33	CYP2C19 inhibitor	No
11	TPSA	20.31	34	CYP2C9 inhibitor	No
	Lipophilicity		35	CYP2D6 inhibitor	No
12	iLOGP	0	36	CYP3A4 inhibitor	No
13	XLOGP3	2.46	37	log Kp (cm/s)	-6.07
			38	CACO-2 (log P{app})	-4.75 cm/s
14	WLOGP	2.16		Druglikeness	
15	MLOGP	2.97	39	Lipinski #violations	0
16	Silicos-IT Log P	2.48	40	Ghose #violations	0
17	Consensus Log P	2.01	41	Veber #violations	0
	Water Solubility		42	Egan #violations	0
18	ESOL Log S	-2.8	43	Muegge #violations	0
19	ESOL Solubility (mg/ml)	3.96E-01	44	Bioavailability Score	0.55
20	ESOL Solubility (mol/l)	1.59E-03		Medicinal Chemistry	
21	ESOL Class	Soluble	45	PAINS #alerts	0
22	Ali Log S	-2.53	46	Brenk #alerts	1
23	Ali Solubility (mg/ml)	7.32E-01	47	Leadlikeness #violations	1
24	Ali Solubility (mol/l)	2.95E-03	48	Synthetic Accessibility	3.88

ADME profiles and drug likeness metrics were assessed utilizing PreADME and SWISSADME online tools for the compound under investigation and are shown in Table I.

The Lipinski rule of 5 (LiR of 5) helps to distinguish between drug-like and non-drug-like molecules. The calculated values for drug likeness parameters of the title compound are: (i) HBD is 0 (≤5) (No -OH or -NH groups to hinder desolvation), (ii) HBA is 2 (≤10), (iii) MW is 248.36 g/mol (≤500 g/mol), (iv) MR is 81 (40-130 cm^3 mol^{-1}) and (v) log P is 2.01 (0-5) (vi) number of rotatable bonds is 2 (Rigid structure favors membrane entry), suggesting excellent permeability through biological membranes and advantageous binding to plasma proteins [22-24]. The van der Waals topological polar surface area of the compound is 20.31 $Å^2$ (TPSA-Excellent -Low polarity ensures easy lipid bilayer permeation) which is less than 120 $Å^2$.The partition coefficient (Milog P) is 2.97, which is within the range of ≤5.

In terms of ADME parameters, the human intestinal absorption (HIA) (calculated from integral of MW,HBD, HBA and TPSA), of value represents the combined absorption and bioavailability derived from the excretion through urine, bile, and feces, with a calculated value of estimated at > 90-95% HIA % [25, 26]. CaCo-2 is a cell line derived from human colon epithelial tissue and is frequently used as a model to evaluate drug absorption in the human digestive system. The calculated value of 40.72 nm/s falls within the acceptable range of

[13.0–76.7 nm/s], indicating excellent intestinal absorption. Madin Darby Canine Kidney (MDCK) cells are commonly used in vitro to determine the permeability of drug candidates, offering insights into their potential absorption in the gastrointestinal tract and across the blood-brain barrier. Drug permeability through MDCK cell monolayers is typically measured in nm/s and is used to classify the drug's absorption capacity, as MDCK cells grow faster than CaCo-2 cells [27].The permeability measurement for MDCK cells was found to be 200.4212 nm/s [25–500 nm/s], which is suitable for elimination by renal cells. The computed skin permeability value for MTDPE is -2.77 cm/h (log Kp < -4), indicating that the compound may penetrate the skin. The inability of MTDPE to inhibit CYP2C9, CYP2C19, CYP2D6, and CYP3A4 indicates that the molecule requires xenobiotic metabolism in the body. Typically, a molecule with 10 or fewer rotatable bonds (RBs) is considered to have favorable drug-like properties. MTDPE has only 2 rotatable bonds. In both in vitro and in silico evaluations of drug-like properties, the expected pharmacokinetic parameters and physicochemical characteristics known as Lipinski's rules are important [28, 29].

3.5.Toxicity predictions

Assessing toxicity is crucial in drug development and aids in recognizing harmful effects of new medications on the body. The toxicity of the compound MTDPE was assessed using the ProTox-II online software [30].

Table-II- Prediction of TOXicity of MTDPE USING ProTox-3.0

Classification	Target	Prediction	Probability
Organ toxicity	Hepatotoxicity	Inactive	0.55
Organ toxicity	Neurotoxicity	Active	0.57
Organ toxicity	Nephrotoxicity	Inactive	0.67
Organ toxicity	Respiratory toxicity	Active	0.62
Organ toxicity	Cardiotoxicity	Inactive	0.76
Toxicity end points	Carcinogenicity	Active	0.65
Toxicity end points	Immunotoxicity	Inactive	0.9
Toxicity end points	Mutagenicity	Inactive	0.7
Toxicity end points	Cytotoxicity	Inactive	0.71
Toxicity end points	BBB-barrier	**Active**	0.92
Toxicity end points	Ecotoxicity	Active	0.59
Toxicity end points	Clinical toxicity	Active	0.5
Toxicity end points	Nutritional toxicity	Active	0.5
Tox21-Nuclear receptor signaling pathways	Aryl hydrocarbon Receptor (AhR)	Inactive	0.86
Tox21-Nuclear receptor signaling pathways	Androgen Receptor (AR)	Inactive	0.88
Tox21-Nuclear receptor signaling pathways	Androgen Receptor Ligand Binding Domain (AR-LBD)	Inactive	0.98

Tox21-Nuclear receptor signaling pathways	Aromatase	Inactive	0.84
Tox21-Nuclear receptor signaling pathways	Estrogen Receptor Alpha (ER)	Inactive	0.87
Tox21-Nuclear receptor signaling pathways	Estrogen Receptor Ligand Binding Domain (ER-LBD)	Inactive	0.91
Tox21-Nuclear receptor signaling pathways	Peroxisome Proliferator Activated Receptor Gamma (PPAR-Gamma)	Inactive	0.96
Tox21-Stress response pathways	Nuclear factor (erythroid-derived 2)-like 2/antioxidant responsive element (nrf2/ARE)	Inactive	0.89
Tox21-Stress response pathways	Heat shock factor response element (HSE)	Inactive	0.89
Tox21-Stress response pathways	Mitochondrial Membrane Potential (MMP)	Inactive	0.76
Tox21-Stress response pathways	Phosphoprotein (Tumor Suppressor) p53	Inactive	0.9
Tox21-Stress response pathways	ATPase family AAA domain-containing protein 5 (ATAD5)	Inactive	0.98
Molecular Initiating Events	Thyroid hormone receptor alpha (THRα)	Inactive	0.9
Molecular Initiating Events	Thyroid hormone receptor beta (THRβ)	Inactive	0.85
Molecular Initiating Events	Transtyretrin (TTR)	Inactive	0.77
Molecular Initiating Events	Ryanodine receptor (RYR)	Inactive	0.88
Molecular Initiating Events	GABA receptor (GABAR)	Active	0.51
Molecular Initiating Events	Glutamate N-methyl-D-aspartate receptor (NMDAR)	Inactive	0.96
Molecular Initiating Events	alpha-amino-3-hydroxy-5-methyl-4-isoxazolepropionate receptor (AMPAR)	Inactive	0.99
Molecular Initiating Events	Kainate receptor (KAR)	Inactive	1
Molecular Initiating Events	Achetylcholinesterase (AChE)	Inactive	0.67
Molecular Initiating Events	Constitutive androstane receptor (CAR)	Inactive	0.99
Molecular Initiating Events	Pregnane X receptor (PXR)	Active	0.53
Molecular Initiating Events	NADH-quinone oxidoreductase (NADHOX)	Inactive	0.72
Molecular Initiating Events	Voltage gated sodium channel (VGSC)	Inactive	0.76
Molecular Initiating Events	Na+/I- symporter (NIS)	Inactive	0.78
Metabolism	Cytochrome CYP1A2	Inactive	0.94
Metabolism	Cytochrome CYP2C19	Inactive	0.79

Metabolism	Cytochrome CYP2C9	Inactive	0.53
Metabolism	Cytochrome CYP2D6	Inactive	0.62
Metabolism	Cytochrome CYP3A4	Inactive	0.8
Metabolism	Cytochrome CYP2E1	Inactive	0.97

The findings of organ toxicity indicated that MTDPE was forecasted to be hepatotoxic, respiratory, and clinical toxic. The results for toxicity endpoints indicated that MTDPE shows activity regarding the blood-brain barrier, Neurotoxicity, Respiratory toxicity and Carcinogenicity and GABA receptor (0.51). The CNS-active compounds consistently cross the Blood–Brain Barrier (BBB) and produce secondary effects in the CNS [31, 32]. The title compound demonstrated activity for molecular initiation events across all parameters.

IV. Conclusions

Molecular dynamics simulations for the ligand MTDPE has been performed to assess RMSD, RMSF, Rg, SASA and Protein-ligand interactions, and it was concluded these parameters are almost identical for the two ligand-protein complexes. Both protein receptors (5YDJ and 6E1C) exhibit nearly identical structural flexibility patterns when interacting with the ligand MTDPE. This is highlighted by matching, pronounced peak fluctuations reaching 3.0 Å around the residue indices with 60-75 and fluctuates between 0.5 to 2.5 Å before finally settling around 3.0 Å for both receptors, demonstrating that MTDPE drives almost uniform local dynamics across both systems. The Radius of Gyration analysis demonstrates that the ligand MTDPE induces identical structural stabilization in protein receptors 5YDJ and 6E1C, with values converging to a stable 2.92 Å after 90 ns. This conformational tightening is supported by a robust, persistent network of protein-ligand contacts that maintains structural rigidity throughout the trajectory. Molecular docking results indicated that the MTDPE-5YDJ complex exhibited the strongest docking with an interaction energy of -7.0 Kcal/Mol, whereas for the MTDPE-6E1C complex, the interaction energy is calculated as -6.6 Kcal/Mol using Autodock Vina tool. The title compound exhibited promising ADMET characteristics and met Lipinski's drug likeness and MDCK drug criteria. These findings should macadamize the way to the development of additional novel biologically active compounds that contain Ethanone rings.

References

[1]. Mehdi S. H., Ghalib R. M., Hashim R. , da Silva M. F. C. G., Sulaiman O., Murugaiyah V., Marimuthu M. M., Naqvi M., *J. of Mol. Structure*, 1049; 488-493; 2013. DOI:10.1016/j.molstruc.2013.06.049

[2]. Ghorab M.M., Ragab F.A., Heiba H. I., Youssef H.A., El-Gazzar M. G., *Med. Chem. Res.*21 (2012) 1376.

[3]. Bandgar B.P., Gawande S.S., Bodade R.G., Gawande N. M., Khobragade C. N., *Bioorg. Med. Chem.* 17 (2009) 816.

[4]. Riyadh S. M., Farghaly T.A., Abdallah M. A., Abdalla M.M., Abd El-Aziz M. R., *Eur. J. Med. Chem.* 45 (2010) 1042.

[5]. Fioravanti R., Bolasco A., Manna F., Rossi F., Orallo F., Ortuso F., Alcaro S., Cirilli R., *Eur. J. Med. Chem*. 45 (2010) 6135.

[6]. Prakash O., Aneja D. K., Arora S., Sharma C., Aneja K. R., *Med. Chem. Res.* 21 (2012) 10.

[7]. Gavara L., Saugues E., Alves G., Debiton E., Anizon F., Moreau P., *Eur. J. Med. Chem.* 45 (2010) 5520.

[8]. Sharma P. K., Kumar S., Kumar P., Kaushik P., Kaushik D., Dhingra Y., Aneja K.R., *Eur. J. Med. Chem.* 45 (2010) 2650.

[9]. Youssef A.M., White M. S., Villanueva E. B., El-Ashmawy I.M., Klegeris A., *Bioorg. Med. Chem.* 18 (2010) 2019.

[10]. Salo-Ahen, Outi M. H., Ida Alanko, Rajendra Bhadane, Alexandre M. J. J. Bonvin, Rodrigo Vargas Honorato, Shakhawath Hossain, André H. Juffer, Aleksei Kabedev, Maija Lahtela-Kakkonen, Anders Støttrup Larsen, and et al. 2021. Processes 9, no. 1: 71. https://doi.org/10.3390/pr9010071.

[11]. Frisch, M. J.; Trucks, G. W.; Schlegel, H. B.; Scuseria, G.E.; Robb, M. A.; Cheeseman, J. R.; Montgomery, Jr., J.A.; Vreven, T.; Kudin, K. N.; Burant, J. C.; Millam, J. M.; Iyengar, S. S.; Tomasi, J.; Barone, V.; Mennucci, B.; Cossi, M.; Scalmani, G.; Rega, N.; Petersson, G. A.; Nakatsuji, H.; Hada, M.; Ehara, M.; Toyota, K.; Fukuda, R.; Hasegawa, J.; Ishida, M.; Nakajima, T.; Honda, Y.;Kitao, O.; Nakai, H.; Klene, M.; Li, X.; Knox, J. E.; P. Hratchian, H.; Cross, J. B.; Adamo, C.; Jaramillo, J.; Gomperts, R.; Stratmann, R. E.; Yazyev, O.; Austin, A. J.; Cammi, R.; Pomelli, C.; Ochterski, J. W.; Ayala, P. Y.; Morokuma, K.; Voth, G. A.; Salvador, P.; Dannenberg, J. J.; Zakrzewski, V. G.; Dapprich, S.; Daniels, A. D.; Strain,M. C.; Farkas, O.; Malick, D. K.; Rabuck, A. D.; Raghavachari, K.; Foresman, J. B.; Ortiz, J. V.; Cui, Q.; Baboul, A. G.; Clifford, S.; Cioslowski, J.; Stefanov, B. B.; Liu, G.; Liashenko, A.; Piskorz, P.; Komaromi, I.; Martin, R. L.; Fox, D. J.; Keith, T.; Alâ€Laham, M. A.; Peng, C. Y.; Nanayakkara, A.; Challacombe, M.; Gill, P. M. W.; Johnson, B.; Chen, W.; Wong, M. W.; Gonzalez, C.; Pople, J. A. et al., Gaussian 09, revision A. 02, Gaussian, Inc., Wallingford CT, 2009.

[12]. Becke, A.D. J. Chem. Phys. 1993, 98, 5648.

[13]. Hohenberg, P.; Kohn, W. Phys. Rev. B. 1964, 136, 864.

[14]. Lee, C.; Yang, W.; Parr, R. G. Phys. Rev. B. 1988, 37, 785.

[15]. Frisch, A. et al. Gaussian Inc. GaussView, Version 6;2009.

[16]. Daina, A.; Michielin, O.; Zoete, V.; SWISSADME online software. 2017.

[17]. Bisong, E. (2019). Google Colaboratory. Apress, Berkeley, CA. 59–64, 2019. https://doi.org/10.1007/978-1-4842-4470-8_7.

[18]. Trott, O.; Olson, A. J. J. Comp. Chem. 2010, 31, 455.

[19]. The PyMOL Molecular Graphics System, Version 1.5.0.4 Schrödinger, LLC.

[20]. Poroikov V.V. Computer-aided drug design: From discovery of novel pharmaceutical agents to systems pharmacology. Biochemistry (Moscow), Supplement Series B: Biomedical Chemistry, 2020, 14(3), 216–227. DOI: 10.1134/S1990750820030117

[21]. http://www.rcsb.org/pdb/explore.do?structureId=5YDJ and 6E1C.
[22]. Valdés-Tresanco, M. S.; Valdés-Tresanco, M. E.; Valiente, P. A.; Moreno, *E. J. Chem. Theory Comput.* 17, 6281, 2021.
[23]. Rudik A., Dmitriev A., Lagunin A., Filimonov D., Poroikov V. *Bioinformatics*, 31 (12), 2046-2048 (2015).
[24]. Ertl, P.; Rohde, B.; Selzer, P. J. Med. Chem. 2000, 43, 3714.
[25]. Murugavel, S.; Ravikumar, C.; Jaabil, G.; Alagusundaram, P. J. Mol. Str. 2019, 1176, 729.
[26]. Veber, D. F.; Johnson, S. R.; Cheng, H. Y.; Smith, B. R.; Ward, K. W.; Kopple, K. D. J. Med. Chem. 2002, 45, 2615.
[27]. Zhao, Y. H.; Le, J.; Abraham, M. H.; Hersey, A.; Eddershaw, P. J.; Luscombe, C. N.; Boutina, D.; Beck, G.; Sherborne, B.; Cooper I.; Platts, J. A. J. Pharm. Sci. 2001, 90, 749.
[28]. Yamashita, S.; Furubayashi, T.; Kataoka, M.; Sakane, T.; Sezaki H.; Tokuda, H. Eur. J. Pharm. Sc. 2000, 10, 195.
[29]. Rodić, M. V.; Leovac, V. M.; Jovanović, L. S.; Spasojević, V.; Joksović, M. D.; Stanojković, T.; Matić, I. Z.; Vojinović-Ješić L.S.; Marković, V. Eur. J. Med. Chem. 2016, 115, 75.
[30]. Lipinski, C. A.; Lombardo, F.; Dominy, B. W.; Feeney, P. J. Adv. Drug Deliv. Rev. 1997, 23, 3.
[31]. Lipinski, C. A. Drug Discov. Today Technol. 2004, 1, 337.
[32]. Gadaleta, D.; Vukovic, K.; Toma, C.; Lavado, G. J.; Karmaus, A. L.; Mansouri. K.; Kleinstreuer, N. C.; Benfenati, E.; Roncaglioni, A. J. Cheminf. 2019, 11, 58.